E# 252

FERMILAB-CONF-74-130-E
COO-3065-60
UR-461

Study of pp Interactions at 102 and 405 GeV/c*

D. Cohen+

Department of Physics and Astronomy

University of Rochester

Rochester, New York 14627

AEC Contract Number AT(11-1)-3065

Paper presented at the Fourth International Symposium on Multiparticle Hadrodynamics, Pavia, Italy, September 1973.

*Research supported by the U. S. Atomic Energy Commission.

+Presently at Nevis Laboratories, Columbia University, P.O.Box 137, Irvington, N.Y. 10533

The data I'm going to discuss are derived from exposures of the National Accelerator Laboratory 30-inch hydrogen bubble chamber which yielded ~5000 pp interactions at 102 GeV/c and ~2500 pp interactions at 405 GeV/c. The entire analysis was performed by the Michigan-Rochester collaboration[1].

I. The Charged-Particle Multiplicity Distribution

Figure 1 shows the measured topological cross sections at 102 GeV/c[2] as well as our preliminary results at 405 GeV/c. The two-prong topology includes only the inelastic events, and its error reflects systematic as well as statistical uncertainties. All other errors are statistical only. In order to distinguish between elastic and inelastic events, all two prongs were fitted to elastic interpretations using the kinematical fitting program SQUAW[3]. In these fits we used the nominal value of the beam momentum for both the incident and the fast outgoing tracks. Our results for the slope of the elastic t distribution at small t values derived from this fitting procedure at both 102 and 405 GeV/c, as well as our values for the total elastic cross section are in good agreement with the more precise counter measurements available. The most salient features of Fig. 1 are the broadening of the multiplicity distribution as the energy increases and the shift of the peak of the distribution to higher multiplicities.

In Fig. 2 we present our values for the mean number of charged particles produced per inelastic pp collision, $\langle n \rangle$, and the Mueller correlation parameters[4] for negative particles given by

$$f_2^- = \langle n_- \ (n_- - 1) \rangle - \langle n_- \rangle^2$$

and

$$f_3^- = \langle n_- \ (n_- - 1)(n_- - 2) \rangle - 3\langle n_- \rangle\langle n_- (n_- - 1) \rangle + 2\langle n_- \rangle^3$$

where n_- is the number of negative particles produced in an interaction. I also show other bubble chamber measurements of these parameters at 50, 69, 205 and 303 GeV/c [5]. The measurements of $\langle n \rangle$ (Fig. 2a) in the 50 to 405 GeV/c momentum range appear to lie on a straight line as a function of $\ell n\ s$, where s is the square of the center of mass energy; however, the χ^2 for the fit to a linear dependence on $\ell n\ s$ is poor. The addition of a $(\ell n\ s)^2$ term does not do much to improve the fit, indicating that there are further systematic discrepancies in the measurements which are not reflected in the quoted errors.

With our new measurements at 102 and 405 GeV/c we can clearly state that the variation of f_2^- between 50 and 405 GeV/c (Fig. 2b) is not consistent with a simple $\ell n\ s$ behavior as predicted by models exhibiting only short-range correlations, i.e., pure multiperipheral models. Previously, the data were consistent with a $\ell n\ s$ behavior, but now a significant $(\ell n\ s)^2$ term is necessary to describe the energy dependence of f_2^- above 50 GeV/c as shown in Fig. 2b. This $(\ell n\ s)^2$ behavior indicates the presence of substantial long-range correlation effects. The energy variation of the f_3^- moment is at present adequately described by a $\ell n\ s$ behavior (Fig. 2c). The statistical errors, however, are still too large to be able to discern a $(\ell n\ s)^2$ dependence. The trend of the data does seen to indicate that f_3^- is heading towards positive values.

Other moments of the multiplicity distribution have also been studied quite extensively. In particular, Wroblewski[6] has noted that the dispersion of the charged-particle multiplicity distribution given by $D = [\langle n^2 \rangle - \langle n \rangle^2]^{\frac{1}{2}}$ appears to follow the functional form $D = 0.58 (\langle n \rangle - 1)$ in pp collisions over a range of beam momenta extending from 4 GeV/c to 303 GeV/c. He has also noted that the skewness and kurtosis

of the distribution defined as

$$\gamma_1 = \frac{\langle (n - \langle n \rangle)^3 \rangle}{D^3}$$

and

$$\gamma_2 = \frac{\langle (n - \langle n \rangle)^4 \rangle}{D^4}$$

respectively, appear to be constant from 12 GeV/c to 303 GeV/c. Koba, Nielsen, and Olesen (KNO)[7], within the framework of their semi-inclusive scaling prediction for the topological cross sections, predicted that the ratios of moments

$$C_q = \frac{\langle n^q \rangle}{\langle n \rangle^q} \qquad q = 2,3,4,\ldots$$

should be a constant. About a year ago Slattery[8] showed that the data available at that time were consistent with the validity of the KNO prediction above 50 GeV/c.

Figure 3 re-examines these moments in light of the presently available data. Figure 3a shows $\langle n \rangle/D$ as a function of $\langle n \rangle$. The KNO prediction is that $\langle n \rangle/D$ should be a constant, and indeed Slattery's fit of last year indicated that it had approached the constant value of 2. The new data clearly indicate that $\langle n \rangle/D$ has not, as yet, approached a constant value, in violation of the KNO prediction, but seems to be following the general trend of the Wroblewski curve. The errors on γ_1 and γ_2 are quite large, and it is therefore difficult to draw any firm conclusions about their behavior. The trend of the data indicates that they might be starting to increase (Figs. 3b and 3c). C_2 and C_3 are shown in Figs. 3d and 3e, and again the constant prediction for these quantities of KNO is clearly violated. The data follow more closely the solid curves which are a result of assuming Wroblewski's

relationship for D as a function of <n>and a constant γ_1.

Thus, the new data from 50 to 405 GeV/c indicate that <n> can be described by a ℓn s behavior while f_2^- shows a substantial $(\ell n\ s)^2$ dependence. At present f_3^- can be adequately described by a ℓn s term only. The moments of the multiplicity distribution clearly indicate that KNO scaling has not as yet set in, but might be approached as $1/\langle n \rangle$.

II. The Diffractive Component in pp Collisions

We have also carried out a study of the reaction

$$pp \rightarrow p + \text{anything}$$

at 102[9] and 405 GeV/c. Our data sample for the above reaction is restricted to protons with values of lab momenta less than 1.2 GeV/c, since these protons can easily be distinguished from pions by ionization. When coupled with a cut on the square of the transverse momentum of the proton of 0.6 $(GeV/c)^2$, this momentum cut yields an unbiased sample of protons for $-1.0 < x < -0.6$, where $x = 2p_\ell^{cm}/\sqrt{s}$ with p_ℓ^{cm} being the center of mass longitudinal momentum of the proton and s the square of the center of mass energy. Since $M^2 \simeq m_p^2 + s(1 - |x|)$, where M is the mass of 'anything' recoiling against the proton and m_p is the proton mass, we see that our cuts yield an unbiased data sample for $M^2 < 80\ GeV^2$ at 102 GeV/c and $M^2 < 320\ GeV^2$ at 405 GeV/c.

Figure 4 displays the x distribution of the proton at 102 and 405 GeV/c excluding the elastic events by the method described earlier. The 405 GeV/c data are, as mentioned earlier, preliminary. The most prominent structure, present at both energies, is the sharp peak near $x = -1$. This peak is

presumably due to diffractive dissociation of the beam proton, with the target proton remaining intact. The peak appears to change in shape somewhat with energy - it appears to have become sharper at 405 GeV/c with the peak moving closer to $x = -1$ and the maximum value of the peak increasing substantially. It is thus clear that this distribution does not scale for $x < -0.95$. If we make the arbitrary definition of calling those events with $-1.0 < x < -0.9$ diffractive events, we see from the integrated cross sections displayed in Fig. 4 that the diffractive cross-section remains constant at a value of ~3 mb as one goes from 100 to 400 GeV/c. The total single diffractive cross section is, of course, twice this number, i.e., ~6 mb. We also note that, beyond the diffractive region, the x distribution scales between 100 and 400 GeV/c. This is clear both from the x distribution and from the integrated cross sections shown in Fig. 4. Our statistical uncertainties are such, however, that we cannot preclude a violation of scaling in this region of ~7%. We note that to obtain an invariant cross section it is simply necessary to multiply each point in the x spectrum by its x value, and thus our conclusions regarding scaling are applicable to the invariant cross section as well.

Figure 5 shows the x distribution of the proton as a function of the associated charged-particle multiplicity. The trend noted previously, namely that the 405 GeV/c data exhibit a narrower x peak with the peak moving closer to $x = -1$ and increasing in magnitude, appears to be borne out by each topology separately, especially for 4 prongs and greater. We also note that the magnitude of the diffractive component, subject to our arbitrary definition of $-1.0 < x < 0.9$, appears to have become somewhat smaller in the 2 and 4 prong topologies (see the integrated

cross sections displayed in Fig. 5), while it is increasing for the 6 prongs and greater. Although the statistics are as yet too meager to make any definitive statement, this trend might indicate that the diffractive component in high energy pp collisions exhibits some dependence on the associated topological cross section as a function of energy.

Recently, counter measurements at the ISR and at NAL[10] have noted the existence of a dip in the x distribution of the proton at $x \sim -0.85$. We show in Fig. 6 the invariant cross section integrated over various t regions as a function of x for the 102 GeV/c data, where t is the square of the momentum transfer from the target to the outgoing proton. The dip is clearly not present in the lowest t range, and emerges more and more prominently as the value of t increases. Similar results are obtained at 405 GeV/c as shown in Fig. 7. Since ISR measurements are not feasible below t values of ~ 0.2 GeV^2, the t dependence of this dip has heretofore not been observed. Some of the observed dependence of the invariant cross section on t is due to kinematics, but the presence of two separate contributions to the x spectrum is certainly suggested by this plot,namely, the diffractive peak which dominates at low t and the high-mass continuum which builds up at larger t.

In Fig. 8 we display the data in terms of the square of the missing mass recoiling from the proton, M^2. The $d\sigma/dM^2$ distributions again show prominent diffractive peaks at both energies with the background level dropping substantially from 102 GeV/c to 405 GeV/c (Fig. 8a). Without trying to define a diffractive region in this case, it appears that the cross section corresponding to the low-mass enhancement above a smooth extrapolation of the background appears to remain relatively

unchanged between the two energies. We also note that the average charged-particle multiplicity as a function of M^2 appears to be virtually energy independent as shown in Fig. 8b. At both energies it is characterized by an initial sharp rise for low M^2 values, followed by a levelling off at high values of M^2. The average value of the transverse momentum of the proton (Fig. 8c) also appears to be energy independent, and is at most only weakly dependent on M^2.

III. Inclusive Pion Production and Charged-Particle Correlations

We have also measured a sample of ~1800 inelastic pp interactions at 102 GeV/c in order to study inclusive pion production and correlations. Figure 9 displays the invariant cross section for π^+ and π^- production integrated over transverse momenta as a function of the rapidity, y, defined as $y = \frac{1}{2} \ell n(\frac{E + p_\ell}{E - p_\ell})$; where E and p_ℓ are the energy and longitudinal momentum of the pion, respectively. These spectra have been corrected for K^+, K^-, p and $\bar{p}$ contamination by Monte Carlo technique using the measured proton and neutral strange-particle spectra at 102 GeV/c. For comparison, we show in Fig. 9 similar data on π^- production at 12 GeV/c and 24 GeV/c. We note that the π^- spectra scale in the proton fragmentation region $y_{lab} < 0.5$, while for $y_{lab} > 0.5$ the invariant cross section increases as a function of energy.

Figure 10 shows the center of mass rapidity distribution for π^-'s as a function of the associated charged-particle multiplicity. The trend that is observed is that the almost flat rapidity distribution that one sees for the four prongs becomes more and more sharply peaked near $y_{cm} = 0$ as the multiplicity increases. Thus, particles with low center of mass rapidity are correlated with high multiplicity events, and vice versa,

a particle with a large rapidity tends to be correlated with low multiplicity events. Thus, this figure indicates an obvious long-range correlation effect, that is, observing any one particle gives us probabilistic information about all other particles accompanying it in a particular reaction.

We have also studied the normalized two-particle correlation function defined as

$$R_{12}(y_1,y_2) = \frac{\sigma_{inel}\ \frac{d^2\sigma}{dy_1 dy_2}}{\frac{d\sigma}{dy_1}\ \frac{d\sigma}{dy_2}} - 1 \quad .$$

For correlation studies involving positive particles all identifiable protons and all positive tracks with $p_\ell^{cm} > 4$ GeV/c have been removed. This latter cut removes the fast protons from the data sample. The remaining protons and the small percentage of removed pions should not markedly affect the shape or magnitude of the correlations presented.

We will be comparing our observed correlation functions to a Monte Carlo calculation based on an independent pion emission model which incorporates known information from the single-particle spectra and from the charged-particle multiplicity distribution. The basic assumptions of this model are:

1. Pions have an equal probability to be π^+, π^- or π^o.
2. Baryons have an equal probability to be protons or neutrons.
3. Charge and baryon number are conserved.
4. The charged-particle multiplicity distribution is constrained to the observed one.
5. The pion transverse momentum is generated according to $e^{-8p_T^2}$.
6. The pion rapidity distribution is assumed to be Gaussian with

the variance (σ^2) varying as $1/\sqrt{n_{TOT}}$, where n_{TOT} is the total number of produced particles. The normalization of the widths was chosen such that the sum of the pion energies peaked at $\sqrt{s}/2$.

Our motivation for constructing such a model is simply to see what sort of two-body correlations can be generated by incorporating 'known physics' such as the multiplicity distribution and the single-particle spectra.

Figure 11 shows R_{12} plotted as a function of the rapidity difference between the two particles, $y_2 - y_1$, for all charged pions. In Fig. 11a we show R_{12} for two rapidity cuts in the central region of center of mass rapidity, while Fig. 11b shows R_{12} for two rapidity cuts having $|y_1| > 1$. In these and in all subsequent plots full use has been made of the symmetry of the pp system. We note that the data tend to peak at $y_2 - y_1 = 0$, with the peaking being more pronounced when one of the particles is constrained to the central region of rapidity. The value of $R_{12}(0,0)$ is approximately 0.6 ± 0.08. This number is in excellent agreement with values measured by the Pisa-Stonybrook Collaboration at the ISR[10] at equivalent laboratory momentum > 1000 GeV/c, indicating that there is very little, if any, increase of R_{12} in the central region for small rapidity separations as a function of energy. This observation is consistent with a multiperipheral picture in the central region of rapidity, and is in disagreement with fragmentation model predictions[11].

The solid curves shown in Fig. 11 are the predictions of the model calculation for R_{12}. Although the model does generate significant two-body correlations, it does not produce as strong correlations as the data exhibit. In particular, the model cannot reproduce the strong peaking that the data exhibit at $y_2-y_1 \sim 0$ both in the central rapidity region (Fig.11a) and away from the central region (Fig. 11b).

Figure 12 shows R_{12} for the $\pi^+\pi^-$ data along with the predictions of the model. These data show stronger peaking for small rapidity separations than the charged-pion data shown in Fig. 11 with a value of $R_{12}(0,0) \sim 0.75$. The model again fails to reproduce the strong peaking of the correlation function at $y_2 - y_1 \sim 0$, and is also in poor agreement with the shape of R_{12}, particularly away from the central region of rapidity (Fig. 12b).

Figure 13 shows the $\pi^+\pi^+$ correlation function, and there is again a substantial peak for small rapidity separations in the central region (Fig. 13a) with a value of ~0.4. Away from the central region (Fig.13b) no peaking is discernable at $y_2 - y_1 = 0$, and one finds a rather flat correlation function for $y_2 - y_1 > 0$. The $\pi^-\pi^-$ data shown in Fig. 14 also only show strong peaking for $y_2 - y_1 \sim 0$ in the central region. The peak value here is large again, with a value of ~0.4.

We thus note that the shape and magnitude of the correlation functions are strongly dependent on the charge state of the pions. This is not too surprising in light of the copious $\pi^+\pi^-$ resonance production that exists which has no counterpart in the $\pi^+\pi^+$ and $\pi^-\pi^-$ systems. It is also clear that a model incorporating only features present in the single-particle spectra and the multiplicity distribution cannot account for the strong correlations that exist in the data. The observed strong correlations for small rapidity separations can be interpreted as evidence for additional particle clustering in the production process.

Figure 15 examines transverse momentum correlations. We have plotted the normalized cross section for observing a pair of pions with and angle ϕ between their transverse momenta. The curves are the

predictions of the same model discussed previously, and peak at 180° as required by energy-momentum conservation. Again, we note that the data for unlike charged pions appear to show more structure than for particles of the same charge. Here, however, energy-momentum conservation requires some correlation, and hence the lack of correlation between pions of the same charge is noteworthy. We also note that the transverse correlations become substantially weaker for large rapidity differences between the two particles. Similar transverse correlation effects to those discussed here have been observed at lower energies[12], and are in general consistent with a simple multiperipheral picture of multiparticle production.

We now discuss briefly charge correlations between particles. In Fig. 16a we show the mean number of charged particles produced per inelastic pp collision in the forward hemisphere of the center of mass, $\langle n_C^F \rangle$, as a function of the number of charged particles emitted backward in the center of mass, n_C^B, at both 102 and 205 GeV/c[13]. We note that there is very little correlation observed; the diffractive contributions manifest themselves as the dips observed at the n_C^B values of 1 and 3. Figure 16b investigates the distribution in the number of charged particles produced backward in the center of mass as a function of topology. The four prong topologies show a strong tendency for a 1-3 separation, probably due to the diffractive component in this topology, and there is a suggestion of a 1-5 separation preference in the six prongs at 205 GeV/c. It is seen that for all topologies greater than four prongs the data peak when there are an equal number of particles in each hemisphere. The curves drawn on the 205 GeV/c distributions are the predictions of a multiperipheral model[14] and fit the high multiplicity events reasonably well.

In Fig. 17a, we show the distribution in u, which is defined to be the amount of charge transferred from one hemisphere to the other in a pp collision. It is seen that 0 charge transfer is the dominant configuration, although $|u| = 1$ is also likely, and there is little or no variation in this distribution from 102 GeV/c to 205 GeV/c. This observation tends to rule out a diffractive model proposed by Chou and Yang[15] which predicts that the mean square deviation, $\bar{u}^2$ (see Fig. 17b), of this distribution should increase as $\sqrt{s}$. The other curve shown is the prediction of a multiperipheral model of Quigg and Thomas.[16]

For further details of the 102 and 405 GeV/c experiments, see Refs. 17-20.

I gratefully acknowledge the assistance of my colleagues at the University of Michigan and at the University of Rochester, in particular, C. Bromberg, for their help in preparing this talk. I would also like to thank the organizers of this conference for the extremely fine job they have done, and Prof. L. Foà for providing me sufficient time during his session to present our results.

References:

1. The people involved in these experiments are: J. Chapman, J. Cooper, N. Green, B. Roe, A. Seidl, and J. Vander Velde from Michigan, and C. Bromberg, D. Chaney, D. Cohen, T. Ferbel, and P. Slattery from Rochester.

2. Preliminary results at this energy have been previously presented. See J. Chapman et al., Phys. Rev. Letters 29, 1686 (1972).

3. The elastic separation at 405 GeV/c has only been performed on half the presently-available data sample, and thus the two prong results to be presented at 405 GeV/c come from half the data sample. The whole exposure was used for all other topologies.

4. A. H. Mueller, Phys. Rev. D4, 150 (1971).

5. 50,69 GeV/c: V. V. Amosov et al., Phys. Letters 42B, 519 (1972); 205 GeV/c: G. Charlton et al., Phys. Rev. Letters 29, 515 (1972); 303 GeV/c: F. T. Dao et al., Phys. Rev. Letters 29, 1627 (1972); The two prong inelastic cross section used for the 303 GeV/c data is given in F. T. Dao et al., NAL-Pub-73/22-Exp, UCLA-1072.

6. A. Wroblewski, Lecture given at the XIII Cracow School of Theoretical Physics, Zakopane, 1973, Warsaw Preprint IFD/5/73, to be published in Acta Physica Polonica.

7. Z. Koba, H. B. Nielsen and P. Olesen, Nucl. Phys. B40, 317 (1972).

8. P. Slattery, Phys. Rev. Letters 29, 1624 (1972); Phys. Rev. D7, 2073 (1973).

9. Preliminary results at this energy have been previously presented. See C. Bromberg et al., UMBC 72-14, UR-416.

10. See, for example, J. C. Sens in Proceedings of the Conference on Recent Advances in Particle Physics, to be published by the New York Academy of Sciences.

11. See, for example, M. Jacob in Proceedings of the XVI International Conference on High Energy Physics (National Accelerator Laboratory, Batavia, Illinois, 1972), Vol. 3, p. 373, J. D. Jackson and A. Roberts, eds.

12. S. Stone et al., Phys. Rev. D5, 1621 (1972).

13. R. Engelmann et al., ANL/HEP 7341.

14. D. R. Snider, ANL/HEP 7326.

15. T. T. Chou and C. N. Yang, Phys. Rev. D7, 1425 (1973).

16. C. Quigg and G. Thomas, Phys. Rev. D7, 2752 (1973).

17. Production of γ, Λ^{o}, K_{s}^{o}, $\bar{\Lambda}^{o}$ in pp Collisions at 102 GeV/c, UMBC-73-20/UR-457.

18. Investigation of a Diffractive Component in pp Collisions at 102 and 405 GeV/c, UMBC 73-21/UR-458.

19. Cross Section and Charged Particle Multiplicities at 102 and 405 GeV/c, UMBC 73-18/UR-459.

20. Pion Production in pp Collisions at 102 GeV/c, UMBC 73-19/UR-460.

Figure Captions

1. Topological cross sections at 102 GeV/c and 405 GeV/c.

2. (a) $\langle n \rangle$, (b) f_2^-, (c) f_3^- as functions of $\ell n\ s$. The curves are the results of fits to the data.

3. (a) $\langle n \rangle / D$, (b) γ_1, (c) γ_2, (d) C_2, (e) C_3 as functions of $\langle n \rangle$. The curves are due to Wroblewski (see text).

4. x distributions for protons with lab momenta <1.2 GeV/c and $p_T^2 < 0.6\ (\text{GeV/c})^2$ at 102 GeV/c and 405 GeV/c.

5. x distributions for protons with lab momenta <1.2 GeV/c and $p_T^2 < 0.6\ (\text{GeV/c})^2$ as a function of topology at 102 GeV/c and 405 GeV/c.

6. The invariant cross section integrated over various t regions as a function of x at 102 GeV/c.

7. The invariant cross section integrated over various t regions as a function of x at 405 GeV/c.

8. (a) $d\sigma/dM^2$, (b) $\langle n \rangle$, (c) $\langle p_T \rangle$ as a function of M^2 at 102 GeV/c and 405 GeV/c.

9. $d\sigma/dy$ distributions for π^+ and π^- at 102 GeV/c. The curves are the same distributions at 12 GeV/c and 24 GeV/c.

10. $d\sigma/dy$ distributions for π^- at 102 GeV/c as a function of the associated charged-particle multiplicity.

11. R_{12} for all charged pions at 102 GeV/c. The curves are the results of the model discussed in the text.

12. R_{12} for $\pi^+\pi^-$.

13. R_{12} for $\pi^+\pi^+$.

14. R_{12} for $\pi^-\pi^-$.

15. $\frac{1}{\pi\sigma}\ \frac{d\sigma}{d\phi}$ at 102 GeV/c, where ϕ is the angle between a pair of pions.

16. (a) Mean number of charged particles produced in the forward center of mass hemisphere as a function of the number of charged particles emitted backward in the center of mass at 102 and 205 GeV/c.

(b) Distribution in the number of charged particles produced backward in the center of mass as a function of topology at 102 and 205 GeV/c.

17. (a) Charge transfer distribution at 102 and 205 GeV/c.

(b) Mean squared deviation of the charge transfer distribution as a function of energy. See text for a discussion of the curves.

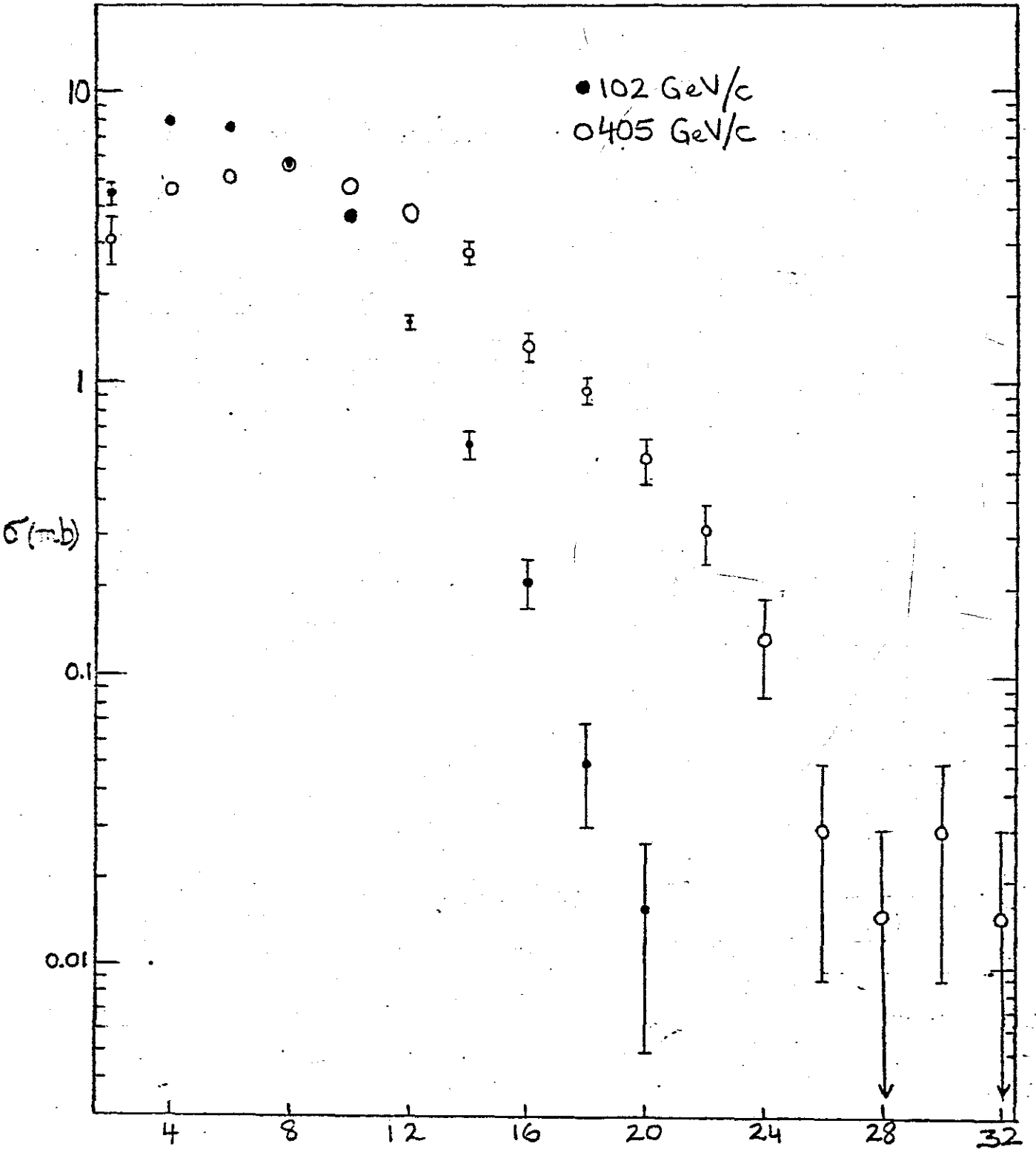
102 GeV/c
405 GeV/c
10
1
0.1
0.01
σ (mb)
4
8
12
16
20
24
28
32
NUMBER OF CHARGED PARTICLES

Fig. 1

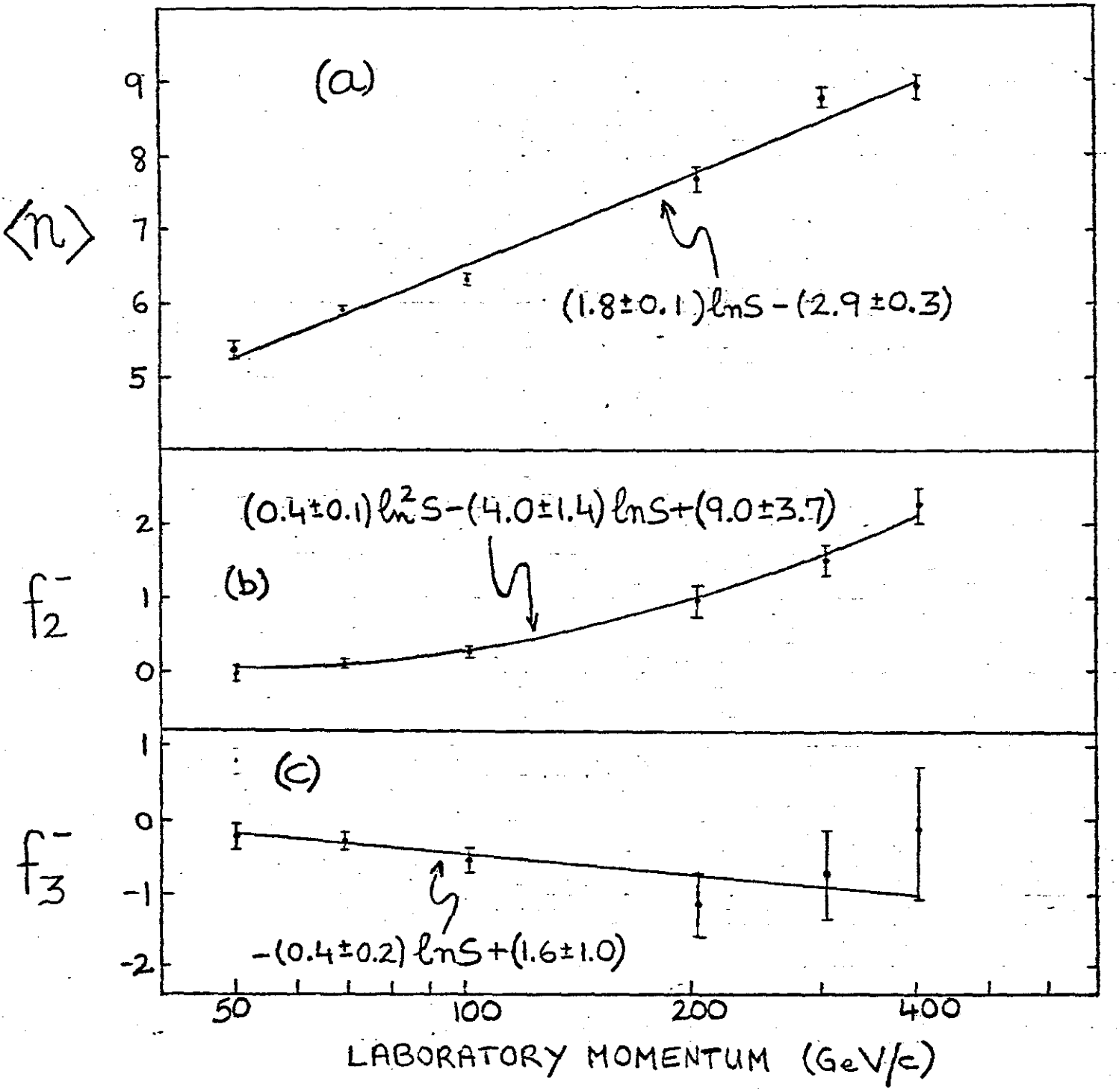
(a)
⟨n⟩
(1.8±0.1) ln S − (2.9±0.3)
(b)
f_2^-
(0.4±0.1) ln²S − (4.0±1.4) ln S + (9.0±3.7)
(c)
f_3^-
−(0.4±0.2) ln S + (1.6±1.0)
LABORATORY MOMENTUM (GeV/c)

Fig. 2

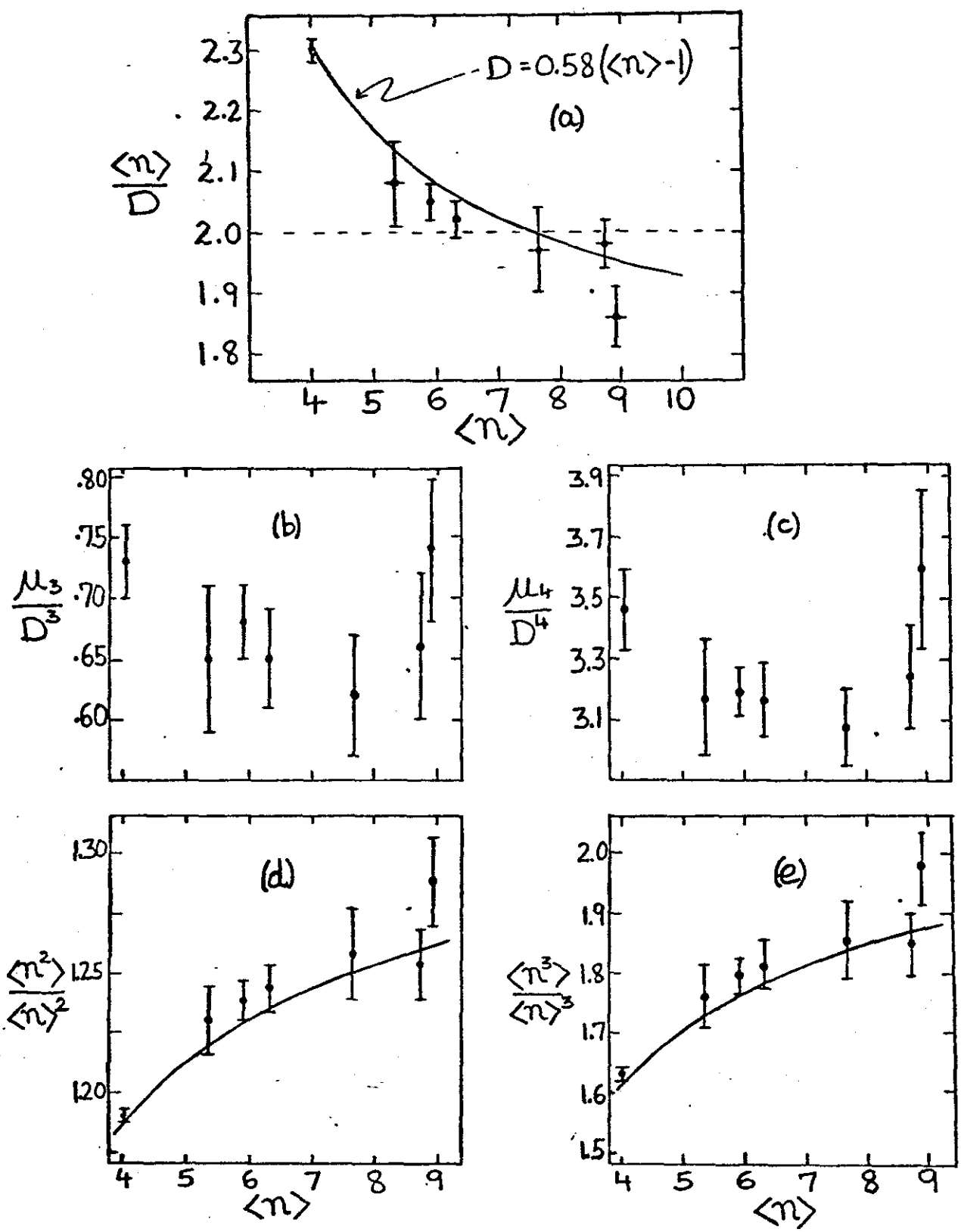

Fig. 3

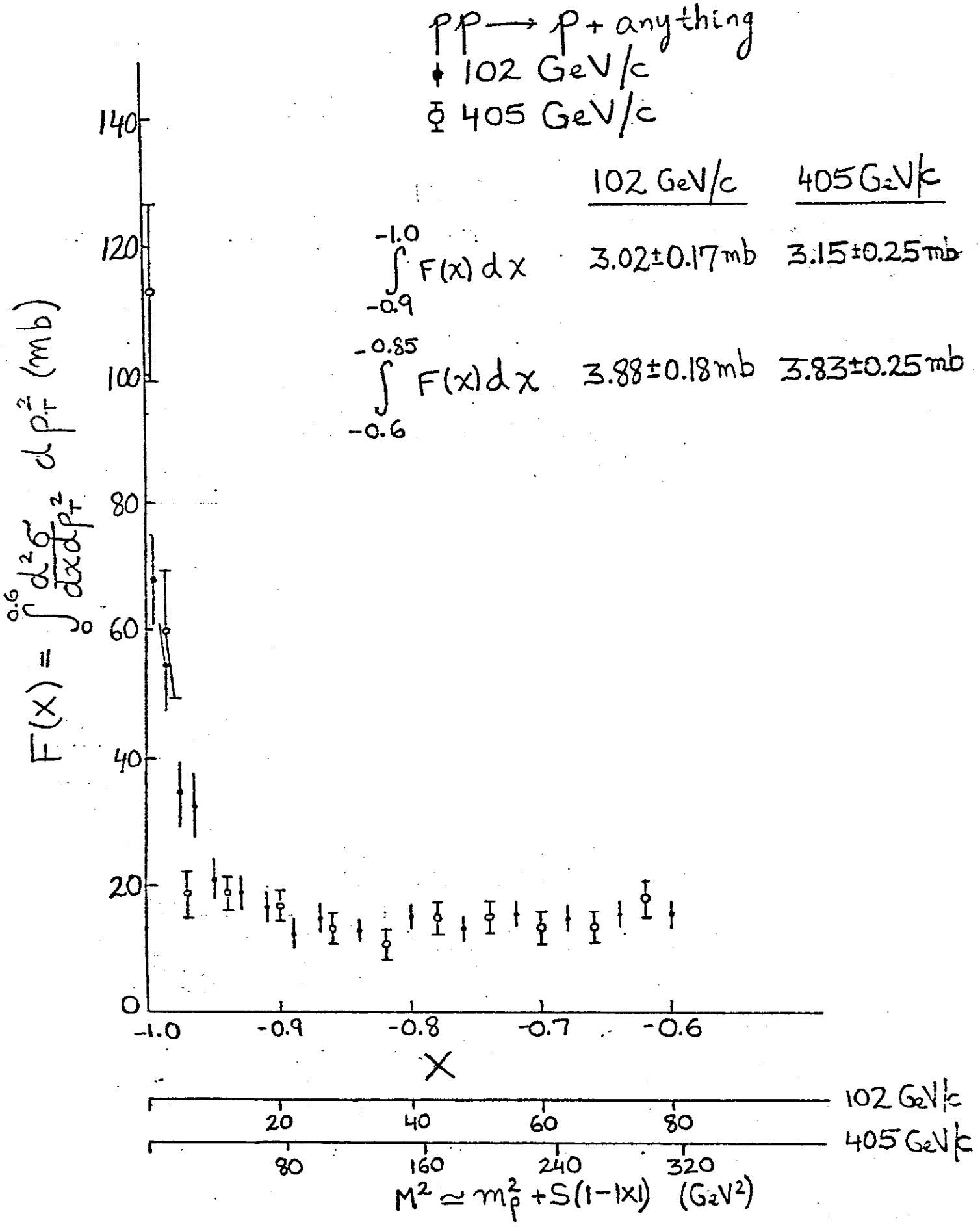
pp → p + anything
102 GeV/c
405 GeV/c
102 GeV/c 405 GeV/c
$\int_{-0.9}^{-1.0} F(x)\,dx$ 3.02±0.17 mb 3.15±0.25 mb
$\int_{-0.6}^{-0.85} F(x)\,dx$ 3.88±0.18 mb 3.83±0.25 mb
$F(x) \equiv \int_0^{0.6} \frac{d^2\sigma}{dx\,dp_T^2}\,dp_T^2$ (mb)
140
120
100
80
60
40
20
0
-1.0
-0.9
-0.8
-0.7
-0.6
X
102 GeV/c
405 GeV/c
20
40
60
80
80
160
240
320
$M^2 \simeq m_p^2 + S(1-|x|)$ (GeV²)

Fig. 4

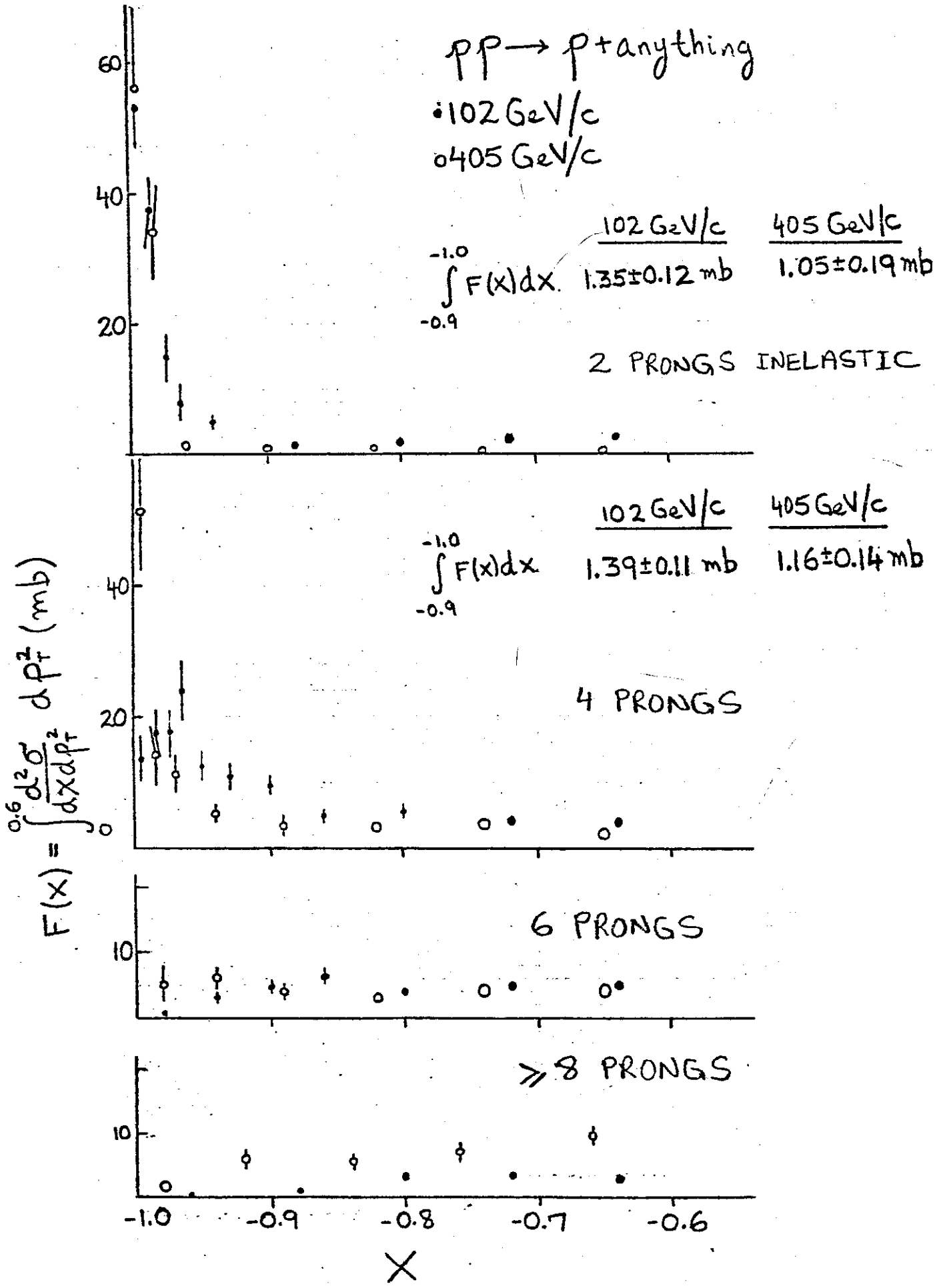
pp → p + anything
• 102 GeV/c
○ 405 GeV/c
102 GeV/c
405 GeV/c
$\int_{-0.9}^{-1.0} F(x)dx$
1.35±0.12 mb
1.05±0.19 mb
2 PRONGS INELASTIC
1.39±0.11 mb
1.16±0.14 mb
4 PRONGS
6 PRONGS
≥8 PRONGS
$F(x) \equiv \int_0^{0.6} \frac{d^2\sigma}{dx\,dp_T^2} dp_T^2$ (mb)
X
60
40
20
10
-1.0
-0.9
-0.8
-0.7
-0.6

Fig. 5

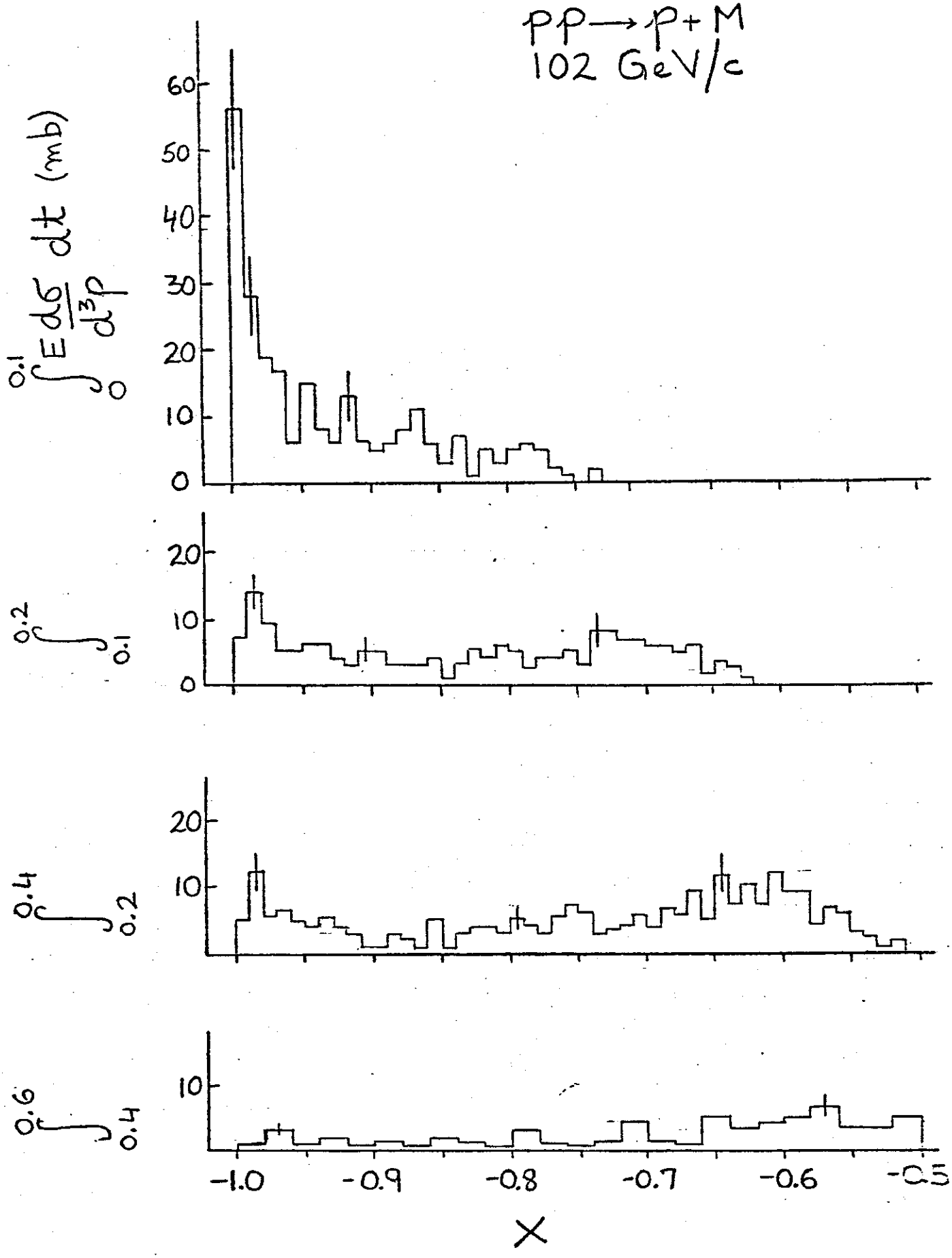
pp → p + M
102 GeV/c
$\int_0^{0.1} E \frac{d\sigma}{d^3p} dt$ (mb)
60
50
40
30
20
10
0
0.2 – 0.1
20
10
0
0.4 – 0.2
20
10
0.6 – 0.4
10
-1.0
-0.9
-0.8
-0.7
-0.6
-0.5
X

Fig. 6

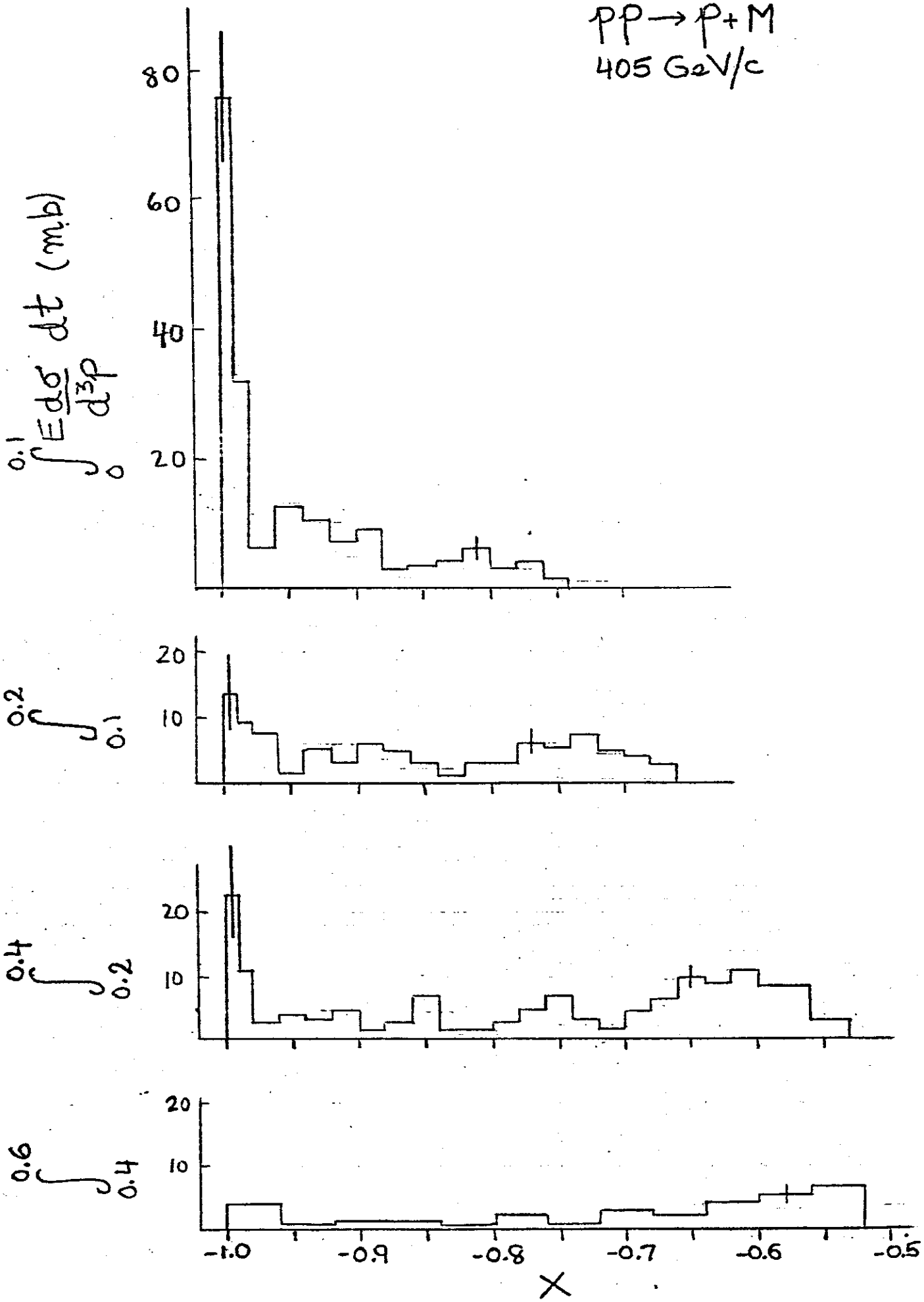
pp → p + M
405 GeV/c
$\int_0^{0.1} E\frac{d\sigma}{d^3p}\,dt$ (mb)
80
60
40
20
$\int_{0.1}^{0.2}$
20
10
$\int_{0.2}^{0.4}$
20
10
$\int_{0.4}^{0.6}$
20
10
-1.0
-0.9
-0.8
-0.7
-0.6
-0.5
X

Fig. 7

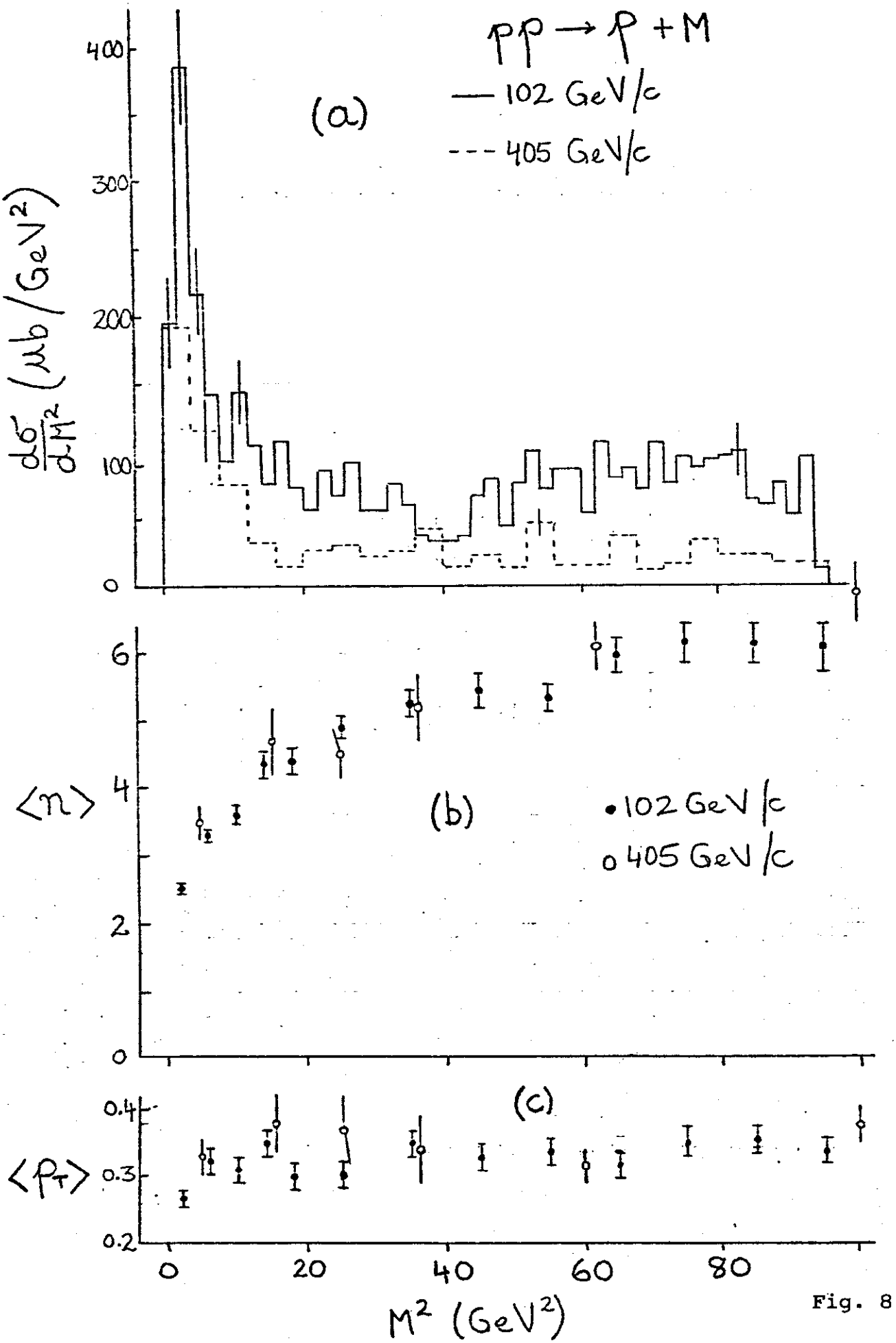
pp → p + M
(a)
— 102 GeV/c
--- 405 GeV/c
dσ/dM² (μb/GeV²)
400
300
200
100
0
(b)
• 102 GeV/c
o 405 GeV/c
⟨n⟩
6
4
2
0
(c)
⟨pT⟩
0.4
0.3
0.2
0
20
40
60
80
M² (GeV²)

Fig. 8

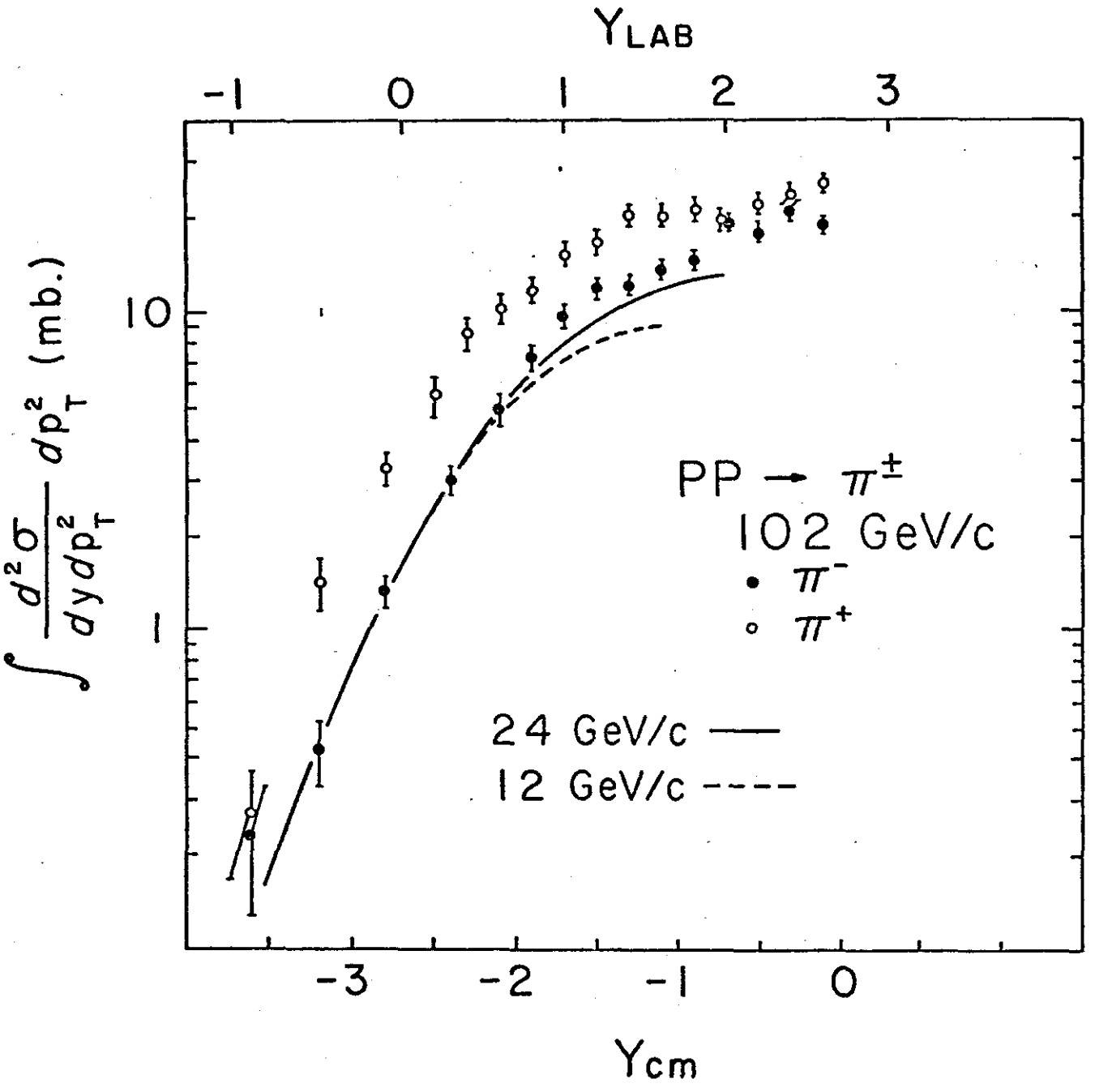
Y_{LAB}
-1
0
1
2
3
10
1
$\int \frac{d^2\sigma}{dy\,dp_T^2}\,dp_T^2$ (mb.)
$PP \rightarrow \pi^{\pm}$
102 GeV/c
$\bullet\ \pi^-$
$\circ\ \pi^+$
24 GeV/c
12 GeV/c
-3
-2
-1
0
Y_{cm}

Fig. 9

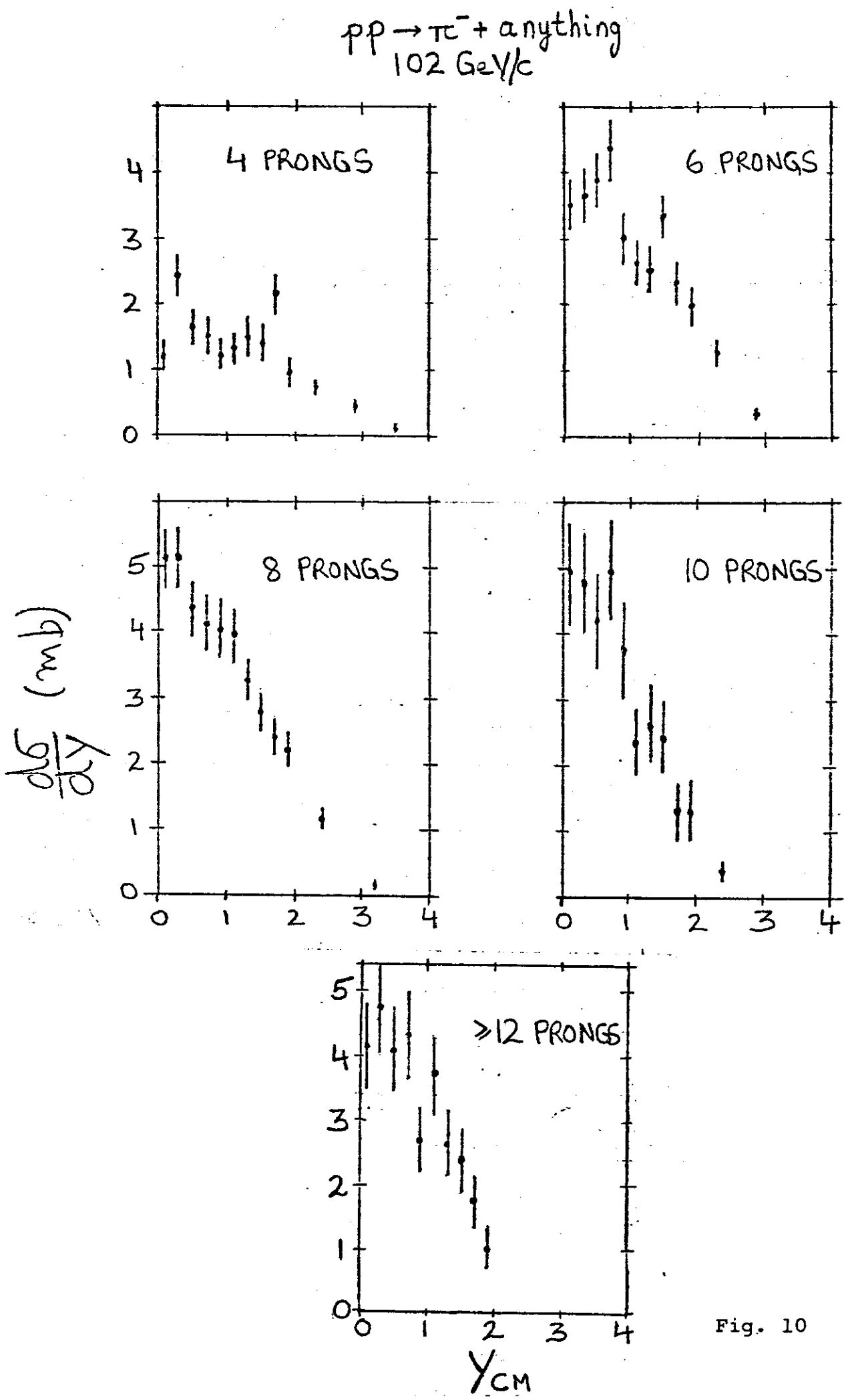
pp → π⁻ + anything
102 GeV/c
4 PRONGS
6 PRONGS
8 PRONGS
10 PRONGS
≥12 PRONGS
dσ/dy (mb)
y_CM

Fig. 10

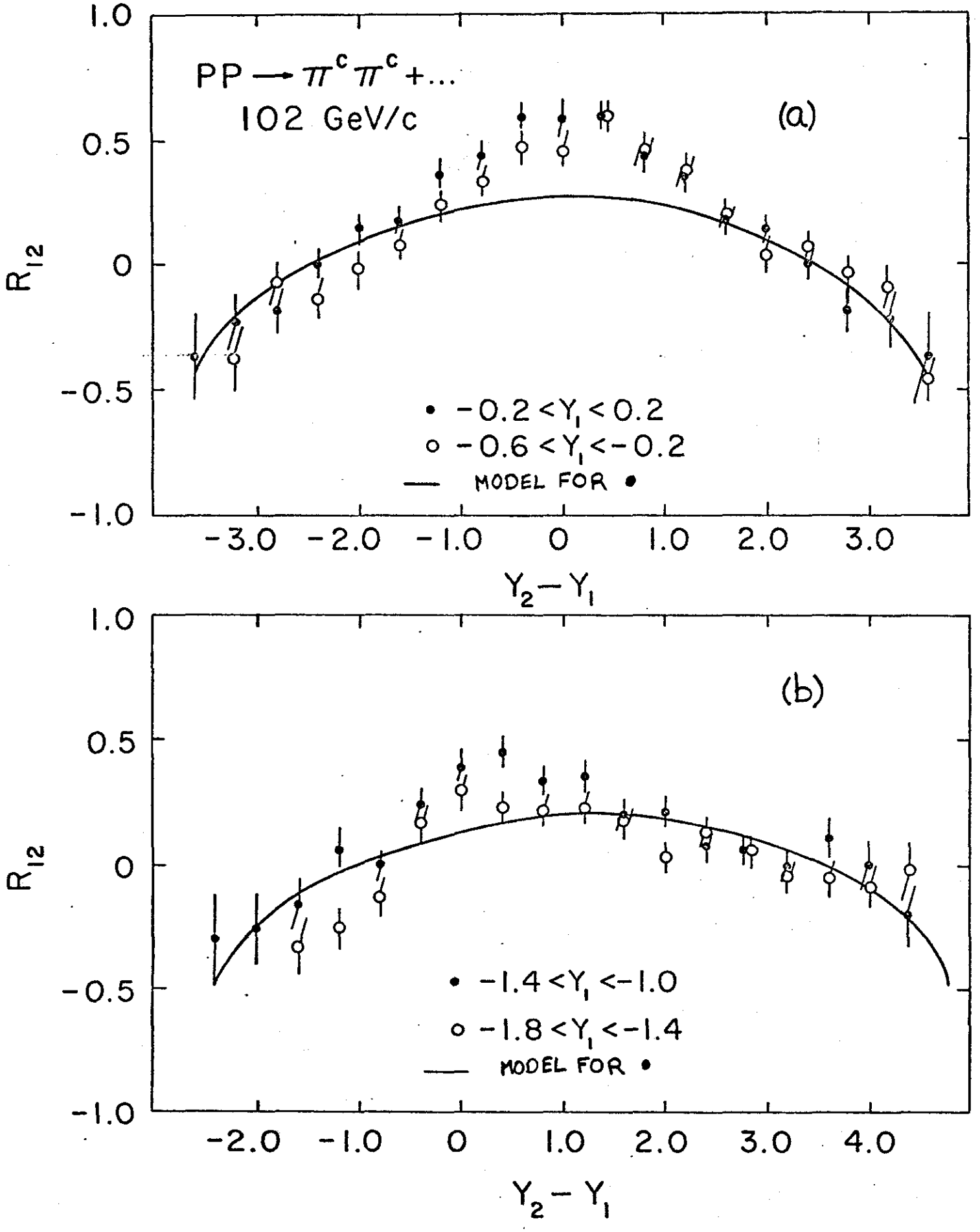
PP → π^c π^c + ...
102 GeV/c
(a)
• −0.2 < Y1 < 0.2
○ −0.6 < Y1 < −0.2
— MODEL FOR •
R12
Y2 − Y1
(b)
• −1.4 < Y1 < −1.0
○ −1.8 < Y1 < −1.4
— MODEL FOR •
R12
Y2 − Y1

Fig. 11

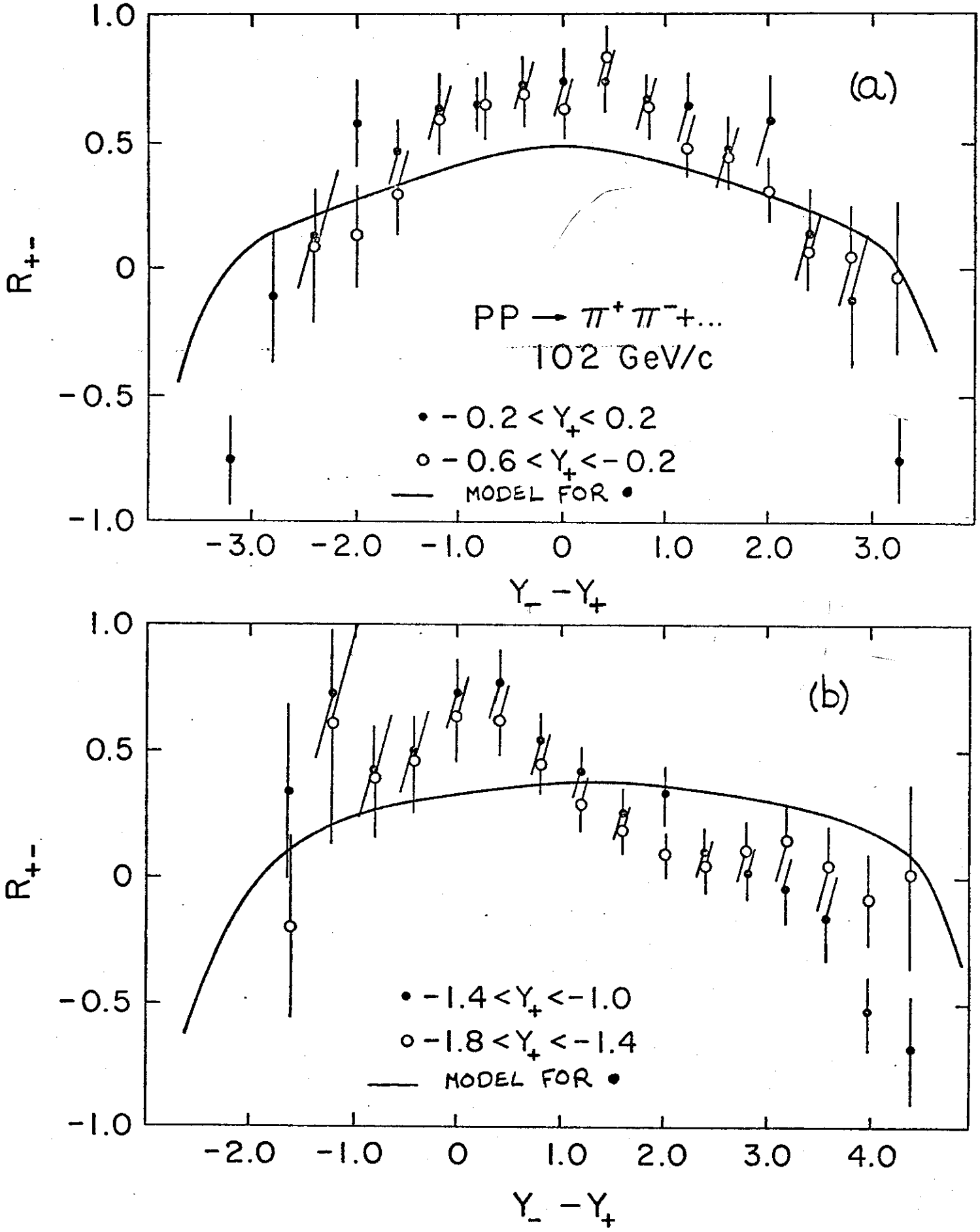
(a)
PP → π⁺π⁻+...
102 GeV/c
• −0.2 < Y₊ < 0.2
○ −0.6 < Y₊ < −0.2
— MODEL FOR •
R₊₋
Y₋ − Y₊
(b)
• −1.4 < Y₊ < −1.0
○ −1.8 < Y₊ < −1.4
— MODEL FOR •
R₊₋
Y₋ − Y₊

Fig. 12

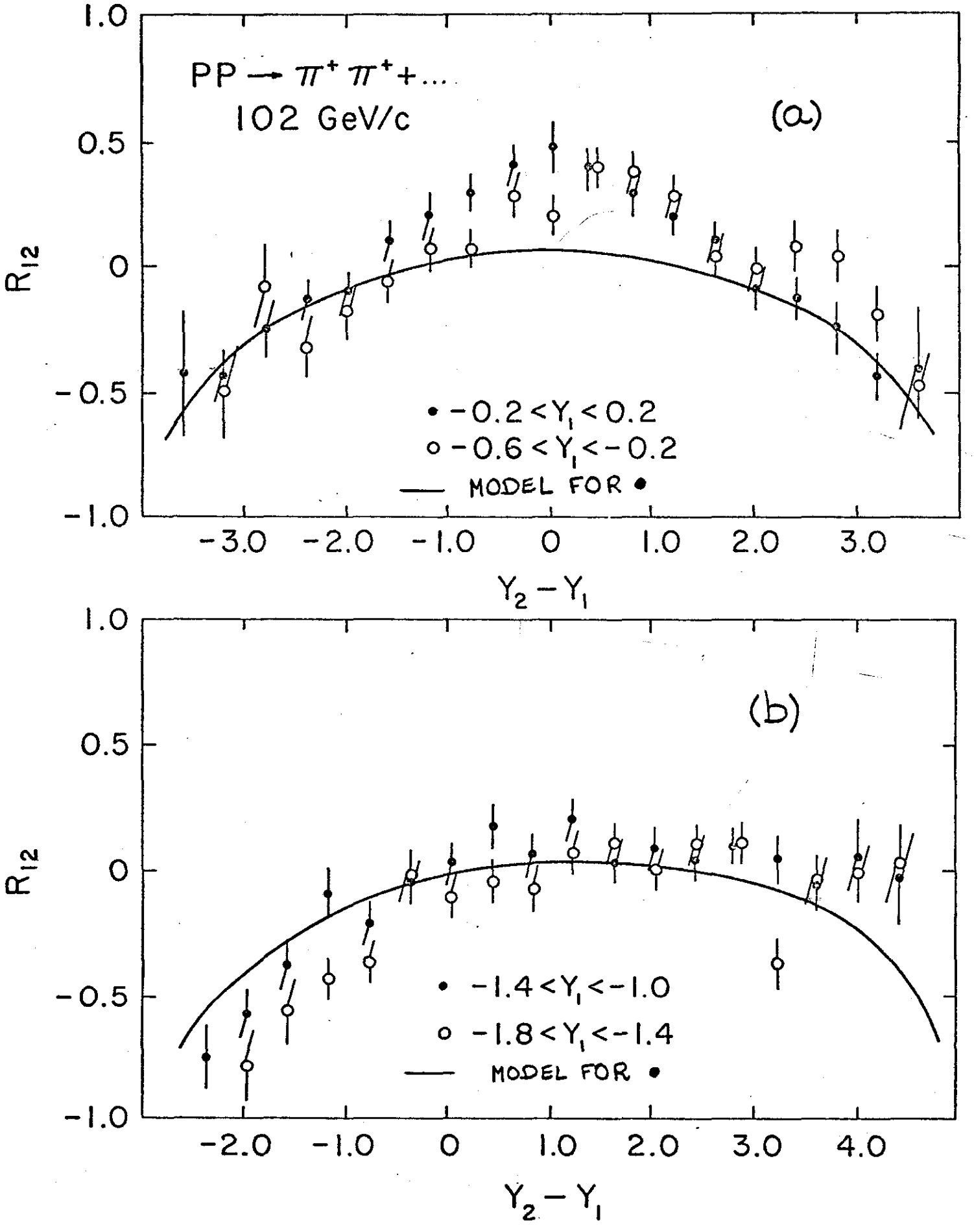
PP → π⁺π⁺+...
102 GeV/c
(a)
• −0.2 < Y₁ < 0.2
○ −0.6 < Y₁ < −0.2
— MODEL FOR •
R₁₂
Y₂ − Y₁
(b)
• −1.4 < Y₁ < −1.0
○ −1.8 < Y₁ < −1.4
— MODEL FOR •
R₁₂
Y₂ − Y₁

Fig. 13

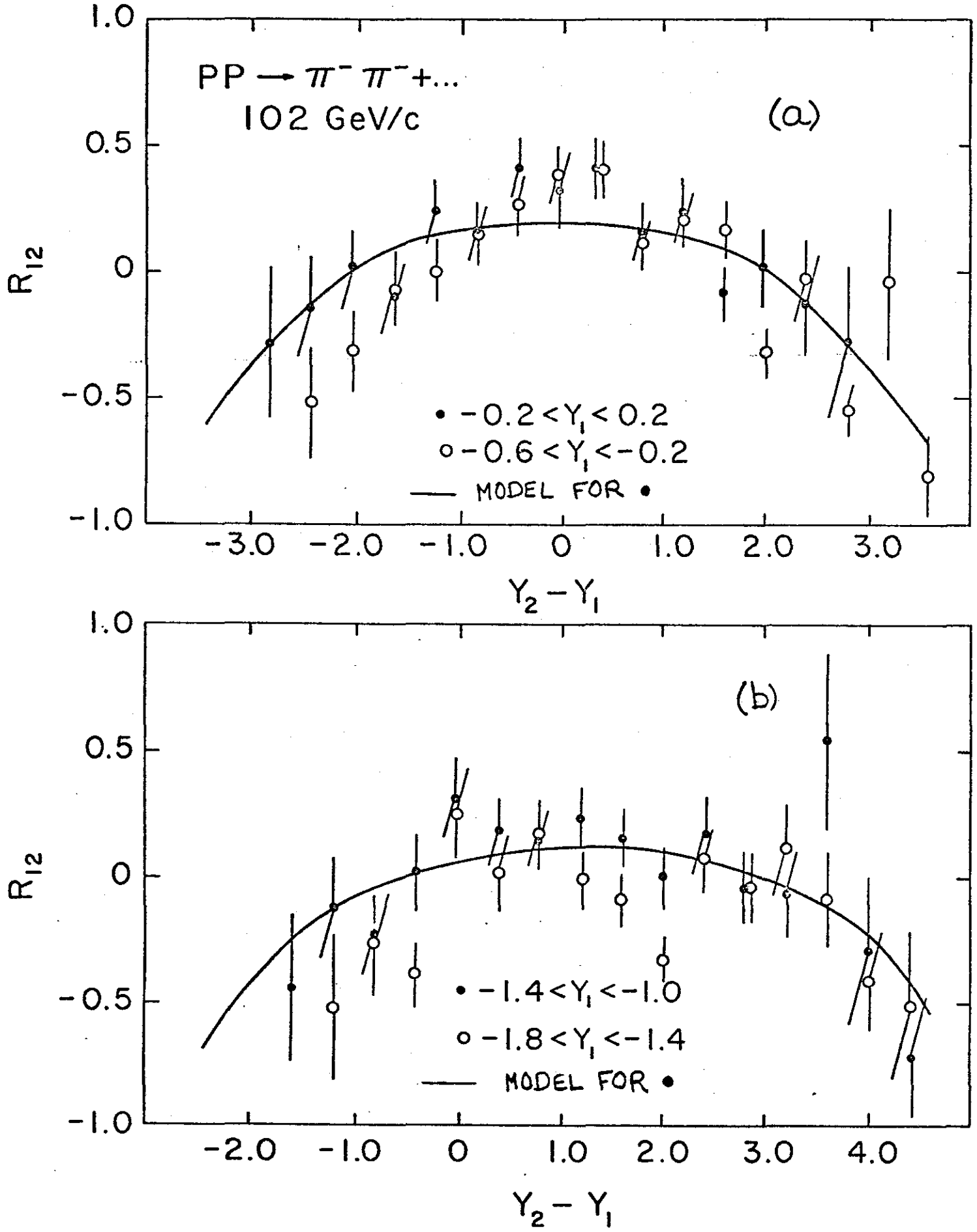
PP → π⁻ π⁻ + ...
102 GeV/c
(a)
• −0.2 < Y₁ < 0.2
○ −0.6 < Y₁ < −0.2
MODEL FOR •
R12
Y2 − Y1
(b)
• −1.4 < Y₁ < −1.0
○ −1.8 < Y₁ < −1.4
MODEL FOR •
R12
Y2 − Y1

Fig. 14

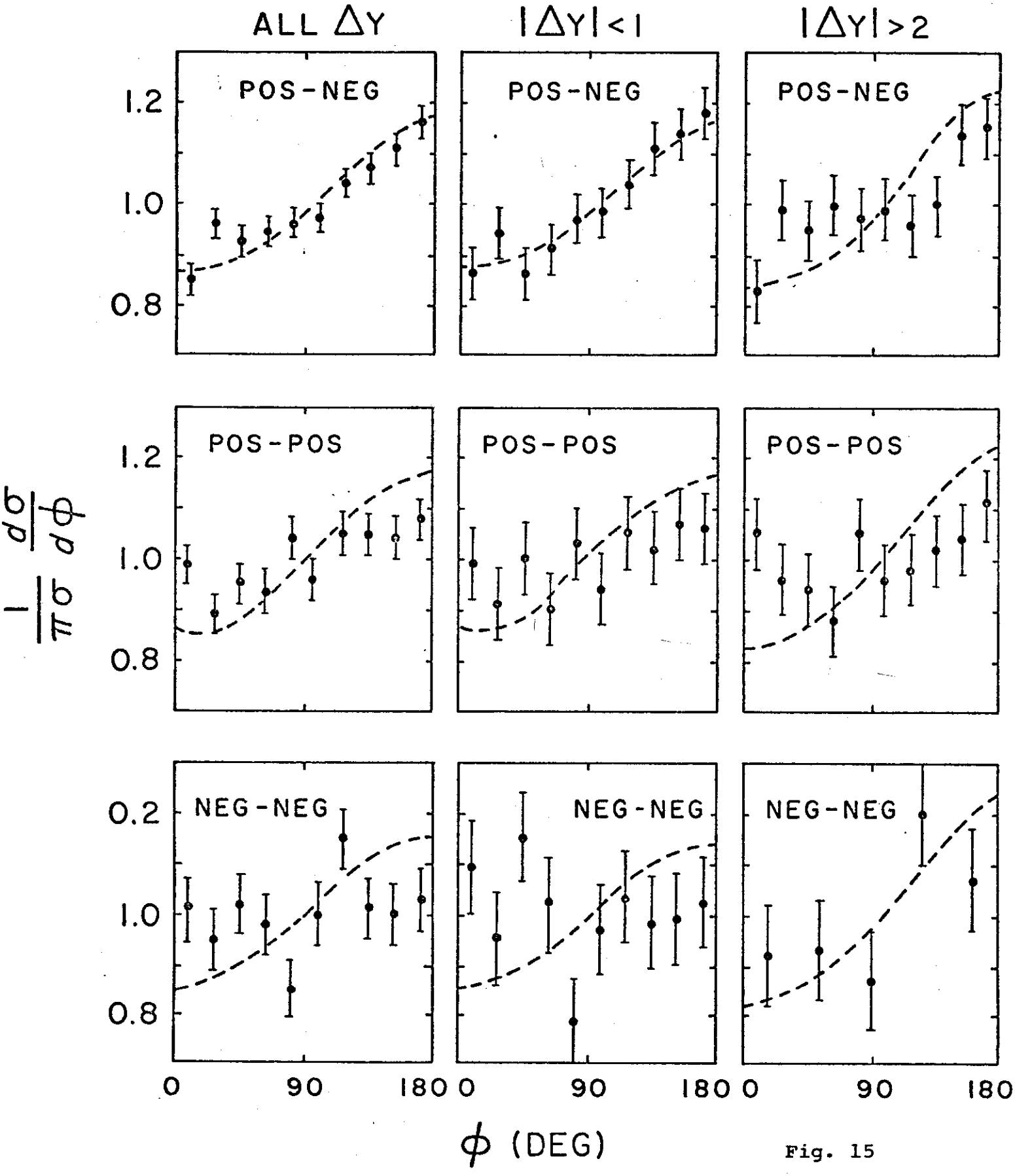

Fig. 15

$n_c > 6$ (PROTONS REMOVED)

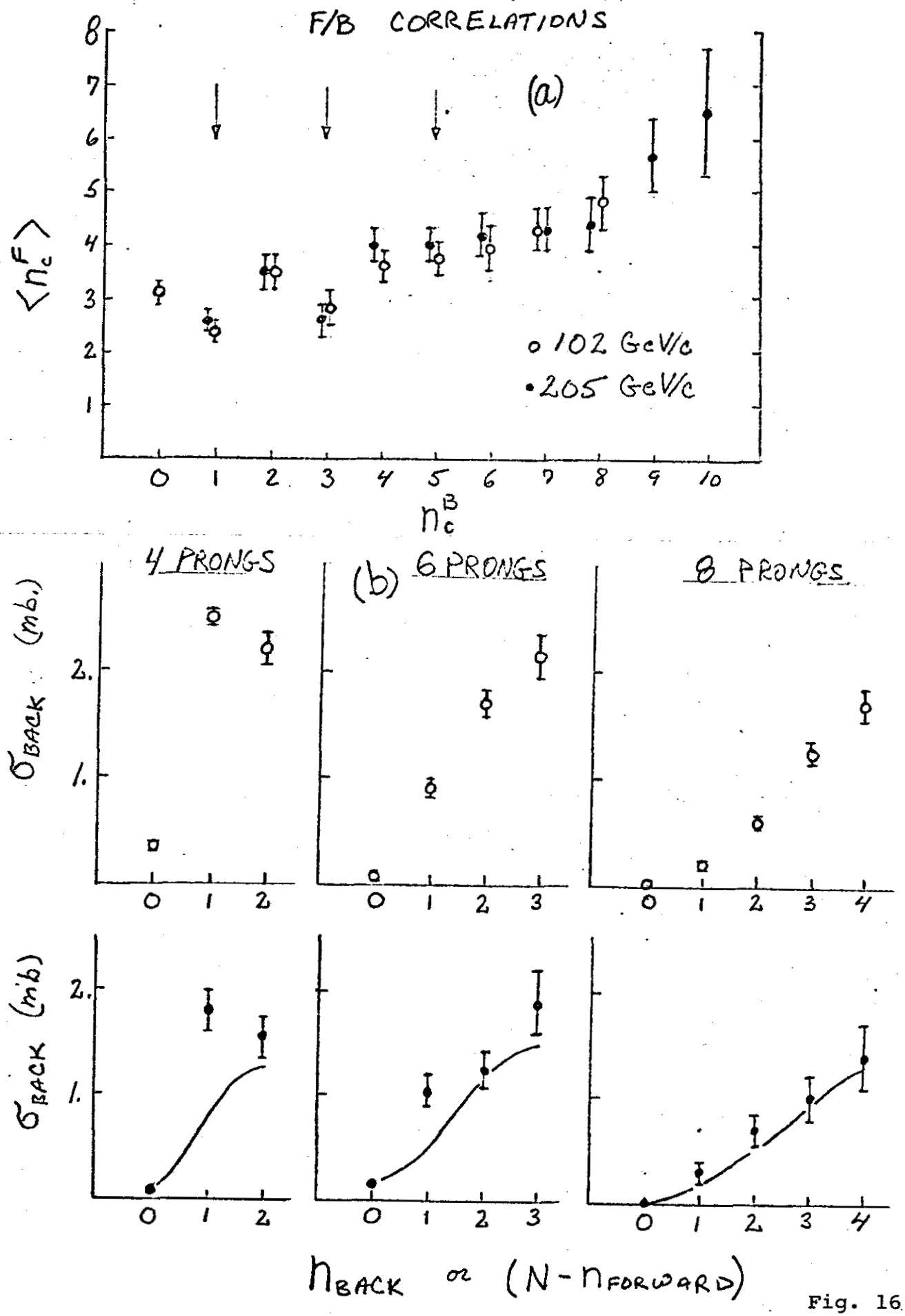
F/B CORRELATIONS
(a)
$\langle n_c^F \rangle$
o 102 GeV/c
• 205 GeV/c
n_c^B
(b)
4 PRONGS
6 PRONGS
8 PRONGS
σ_{BACK} (mb.)
n_{BACK} or $(N - n_{FORWARD})$

Fig. 16

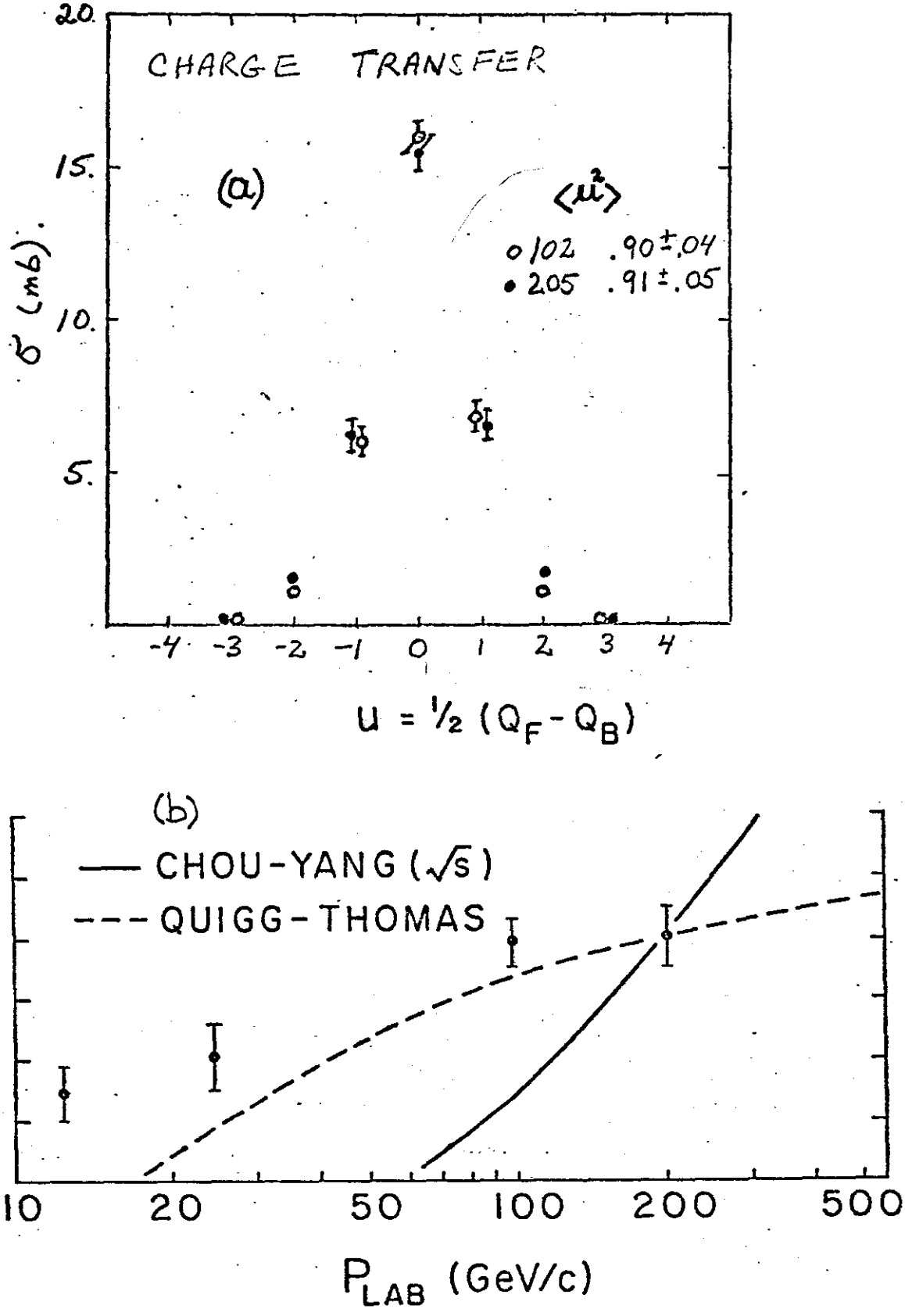
CHARGE TRANSFER
(a)
$\langle u^2 \rangle$
o 1.02 .90 ± .04
• 2.05 .91 ± .05
σ (mb)
20.
15.
10.
5.
-4 -3 -2 -1 0 1 2 3 4
u = ½ (Q_F - Q_B)
(b)
CHOU-YANG (√s)
QUIGG-THOMAS
<u²>
1.0
0.8
0.6
10 20 50 100 200 500
P_LAB (GeV/c)

Fig. 17